Filtering ground noise from LiDAR returns produces inferior models of forest aboveground biomass

Michael J Mahoney[a,*], Lucas K Johnson[a], Eddie Bevilacqua[b], Colin M Beier[b]

[a] *Graduate Program in Environmental Science, State University of New York College of Environmental Science and Forestry, 1 Forestry Drive, Syracuse, New York, 13210*

[b] *Department of Sustainable Resources Management, State University of New York College of Environmental Science and Forestry, 1 Forestry Drive, Syracuse, New York, 13210*

*Corresponding Author (Email Address mjmahone@esf.edu)

**Running head: Filtering ground noise from forest AGB models

This paper is a non-peer reviewed preprint submitted to EarthArXiv prior to publication.

Abstract

1. Airborne LiDAR has become an essential data source for large-scale, high-resolution modeling of forest biomass and carbon stocks, enabling predictions with much higher resolution and accuracy than can be achieved using optical imagery alone. Ground noise filtering – that is, excluding returns from LiDAR point clouds based on simple height thresholds – is a common practice meant to improve the 'signal' content of LiDAR returns by preventing ground returns from masking useful information about tree size and condition contained within canopy returns. Although this procedure originated in LiDAR-based estimation of mean tree and canopy height, ground noise filtering has remained prevalent in LiDAR pre-processing, even as modelers have shifted focus to forest aboveground biomass (AGB) and related characteristics for which ground returns may contain useful information about stand density and openness. In particular, ground returns may be helpful for making accurate biomass predictions in heterogeneous landscapes that include a patchy mosaic of vegetation heights and land cover types.
2. In this paper, we applied several ground noise filtering thresholds while mapping AGB across New York State (USA), a heterogenous landscape composed of both contiguously forested and highly fragmented areas with mixed cover types. We fit random forest models to predictor sets derived from each filtering intensity threshold and compared model accuracies, paying attention to how changes in accuracy correlated with landscape structure.
3. We observed that removing ground noise via any height threshold systematically biases many of the LiDAR-derived variables used in AGB modeling.

We found that that ground noise filtering yields models of forest AGB with lower accuracy than models trained using predictors derived from unfiltered point clouds. Models fit to predictors derived from filtered point clouds performed worse as landscape heterogeneity (as measured by patch density and edge density) increased.

4. Our results suggest that ground filtering should be avoided when mapping biomass, particularly when mapping heterogeneous and highly fragmented landscapes, as ground returns are more likely to represent useful ‘signal’ than extraneous ‘noise’ in these cases.

Keywords: aboveground biomass; ground noise; LiDAR; machine learning; random forest

1. Introduction

Accurate assessment of forest carbon stocks for the purposes of greenhouse gas accounting and climate change mitigation requires high-resolution maps of above-ground biomass (AGB) across large spatial extents. The production of these maps has been aided in recent years by the proliferation of publicly available airborne LiDAR data, allowing researchers access to granular data representing the 3D profile of the earth’s surface at a landscape scale (Dubayah & Drake, 2000). By aggregating returns to a pixel or object level and computing descriptive statistics characterizing the distributions of return heights, modelers are able to convert these point clouds into tabular data formats which may then be used to fit regression models for predicting AGB (Hawbaker et al., 2010).

However, there exists some disagreement about precisely which returns to aggregate when computing such statistics. While some LiDAR-based AGB models include all returns when calculating summary statistics (Hudak et al., 2020), others first filter out returns below various height thresholds when calculating percentile heights (Ma et al., 2018), density percentiles (Huang et al., 2019), or their entire suite of predictors (García et al., 2010). Filtering is typically described as being done to remove ground noise from return data, in order to avoid having "ground" returns mask any signal contained in the remaining "canopy" returns. The height threshold used in this process varies across studies, with examples ranging from 0.3m (García et al., 2010) to 1.3m (Deo et al., 2017; Ma et al., 2018) to 2m (Anderson & Bolstad, 2013) to 2.5m (Huang et al., 2019).

This diversity of approaches demonstrates a lack of consensus about a preprocessing technique that produces systematically greater estimates of percentile heights and other computed predictors. The practice itself appears to have originated with Nilsson (1996), whose early work with airborne LiDAR focused on calculating tree heights based on the maximum heights of returns, as well as stand volume as a function of the mean height of all returns. Nilsson does not appear to filter returns based on height thresholds; rather, they set the height values of all points below 2m to 0m, in effect reducing the resulting mean height values. The following year, Næsset (1997) published what may be the earliest rationale for ground noise filtering in a study calculating mean stand height from LiDAR returns, excluding returns below 2m in order to avoid interference from shrubs, rocks, and other understory features. In concert, these two studies have provided the justification for filtering out ground returns in a multitude of forest modeling studies (Anderson & Bolstad, 2013; Magnussen & Boudewyn, 1998; Wasser et al., 2013), to the extent that it appears to now be such a commonly accepted practice as to not merit discussion or citation at all (Hawbaker et al., 2010; e.g. White et al., 2015).

Yet this practice, initially justified so as to not include the height of stones in calculating the mean heights of trees (Næsset, 1997), may not be necessary or desirable as modelers turn their attention to stand characteristics such as AGB. Increased density of ground returns may be associated with sparser stands, and as a result, the left-censoring of variables derived from LiDAR pulses by omitting ground noise may remove useful information about stand structure available for predictive models. This common practice may therefore result in inferior estimates of forest AGB. Filtering may particularly harm predictive accuracy in less contiguously forested and mixed-use landscapes, as we might expect filtering to exclude more returns in areas without tree canopies intercepting and reflecting pulses. As a result, these filtering procedures may adjust LiDAR-derived variables by greater amounts in these settings compared to contiguously forested regions, given their increased proportion of ground returns. It is likely that modeling such heterogeneous landscapes will be an increasing concern over time, as larger data sets and improved computing power enables modelers to map AGB over larger spatial scales; however, there has not been much discussion in the literature concerning any effects filtering may have on forest AGB predictions either in these landscapes or in more homogeneous settings.

Such a discussion is particularly timely given the current focus on producing high-resolution maps of forest AGB. Numerous studies in recent years have produced such maps using a combination of publicly-available LiDAR and field measurements collected through the United States Forest Service Forest Inventory and Analysis (FIA) program, and despite limitations in LiDAR density and FIA spatial measurement accuracy have produced admirable results. However, such studies may be limiting their success due to this common LiDAR preprocessing procedure.

In this paper, we use publicly-available LiDAR data sets representing a range of contiguously forested and mixed-use landscapes to investigate the impacts of ground noise filtering on predictive models of forest AGB. We set out to first identify how filtering ground noise impacts the distribution of commonly used LiDAR-derived predictors, using multiple height thresholds as found throughout the literature. We then fit models to each of these predictor sets using the random forest algorithm (Breiman, 2001), a popular tool used in modeling AGB, to assess how the different predictor distributions afftected model performance. This study sought to inform current and future efforts looking to accurately predict forest AGB using models incorporating predictors derived from airborne LiDAR data products.

2. Methods

2.1. LiDAR Data Sets and Site Characteristics

In order to identify the impacts of ground filtering on predictive models of AGB, we obtained leaf-off LiDAR data sets flown for sixteen regions across New York State (USA; Figure 1). This data, collected as part of a number of cross-agency federal initiatives, resembles the relatively low-density and leaf-off LiDAR relied upon in similar forest AGB modeling work (see for instance Nilsson et al. (2017), Huang et al. (2019)), and closely resembles the remote sensing data used in typical modeling practice. Data was acquired between 2014 and 2019 and had pulse densities between 1.98 and 3.24 points per square meter. Additional information about individual LiDAR data sets is included as Supplementary Materials S1.

2.2. Field Data

Field measurements of AGB for all trees measuring $\geq$ 12.7 cm diameter at breast height were taken as part of the United States Department of Agriculture (USDA) Forest Inventory and Analysis (FIA) program (Gray et al., 2012), with true macroplot centroid locations obtained under agreement with the USDA. All analyses and models used data aggregated from subplots to the plot level; LiDAR

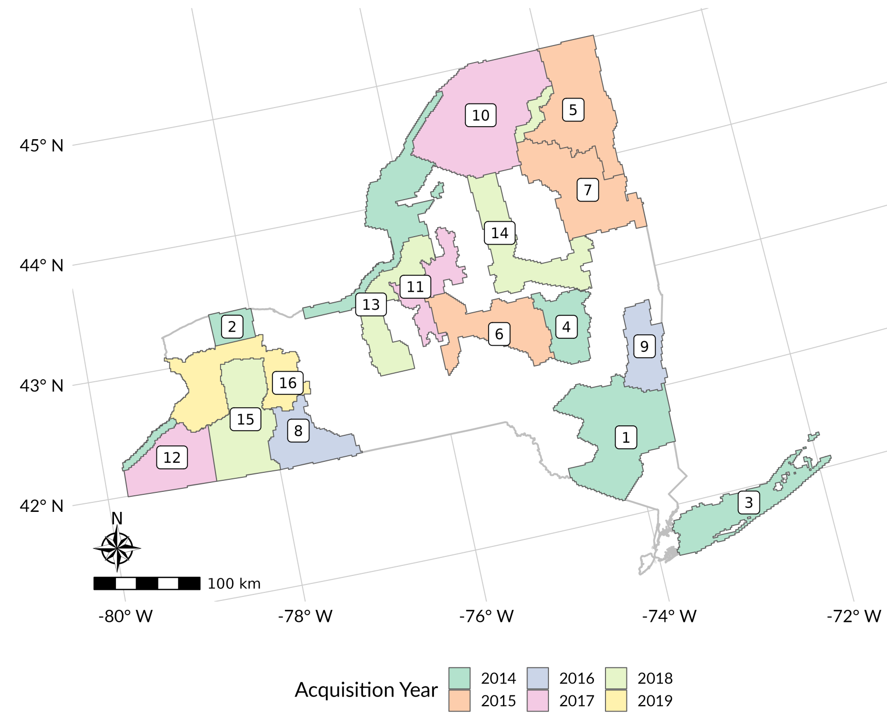

Figure 1: Locations of LiDAR regions within New York State. More information about each region and LiDAR data set is included as Supplementary Materials S1.

data was clipped to only the measured subplot areas, with subplot locations estimated based upon the macroplot centroid, and then pooled prior to predictor derivation. Plots entirely classified as nonforest (which are not assigned biomass by the FIA) were excluded from the dataset. Only FIA plots sampled the same year as LiDAR flights, or FIA plots with measurements both before and after the LiDAR acquisition year with a difference in AGB within [-5%, ∞) (to allow for forest growth or small-scale disturbance) were used for training and evaluating models. In situations where FIA year did not match LiDAR acquisition year, AGB was calculated by linearly interpolating between the values measured in the temporally closest FIA samples. Plots were additionally excluded if any subplots were marked as nonsampled, if FIA measurements indicated 0 Mg ha^{-1} of AGB but maximum LiDAR return heights at the plot exceeded 10 meters, or if the convex hull of all LiDAR returns for a subplot contained less than 90% of the subplot's area. This methodology was chosen to closely resemble the existing literature on forest AGB mapping (see for instance Huang et al. (2019)). AGB measurements were recorded in pounds, then converted and area-normalized to units of megagrams per hectare (Mg ha^{-1}).

2.3. LiDAR Pre-Processing

A digital terrain model (DTM) was calculated for all sites using a k-nearest-neighbors inverse-distance weighting imputation algorithm (using k = 5) as implemented in the lidR R package (Roussel et al., 2020), fit using the points classified as "ground" within the raw LiDAR point cloud data set. The calculated terrain was then subtracted from each point's z value to create a height-normalized point cloud. Ground noise filtering rules were then applied to create five separate points clouds for each site, each representing a different ground noise filtering approach: one point cloud containing all points in the original file (hereafter referred to as "unfiltered"), one removing all points classified as "ground" in the original metadata ("ground," equivalent to a 0m threshold), and three removing all points with normalized z values below a 0.1, 1, or 2 meter threshold ("0.1m," "1m," and "2m," respectively).

Separate sets of 40 predictors, chosen due to their prevalence in published models of AGB and forest structure, were derived from each of these point clouds using the lidR R package (Table 1) (Hawbaker et al., 2010; Huang et al., 2019; Pflugmacher et al., 2012, 2014; Roussel et al., 2020). Predictors computed for FIA plot locations were derived from only the pooled returns coincident with the sampled subplot locations, so as to not include any returns from the unsampled regions of the macroplot. For plots where ground noise filtering resulted in the removal of all points, variables were set to a default value of 0. As highly correlated predictor variables may provide the random forest model less information for AGB predictions, relationships between predictors were assessed using Spearmans's correlation coefficient. Changes in predictor distributions under different filtering methodologies were assessed using Kolmogorov-Smirnov statistics (Massey, 1951).

2.4. Model Fitting

AGB models were fit using the ranger R package's implementation of the random forest algorithm (Breiman, 2001; Wright & Ziegler, 2017), a popular machine learning technique for predicting forest biomass across landscapes (see for instance Huang et al., 2019; Hudak et al., 2020). Separate models were fit on predictors calculated using each level of ground noise filtering ("unfiltered," "ground," "0.1m," "1m," and "2m" thresholds) for each LiDAR region and a combination of all LiDAR regions, for a total of 85 separate models. Each model used data representing all available FIA plots within the relevant LiDAR region (Section 2.2). Models were fit using only LiDAR derived predictors, as it was expected that including non-LiDAR derived variables might mediate and

Table 1: Definitions of LiDAR-derived predictors used for model fitting.

Predictor	Definition
H0, H10, ... H100, H95, H99	Decile heights of returns, in meters, as well as 95th and 99th percentile return heights.
D10, D20... D90	Density of returns above a certain height, as a proportion. After return height is divided into 10 equal bins ranging from 0 to the maximum height of returns, this value reflects the proportion of returns at or above each breakpoint.
N	Number of LiDAR returns clipped to the given FIA plot or map pixel
ZMEAN, ZMEAN_C	Mean height of all returns (ZMEAN) and all returns above 2.5m (ZMEAN_C)
Z_KURT, Z_SKEW	Kurtosis and skewness of height of all returns
QUAD_MEAN, QUAD_MEAN_C	Quadratic mean height of all returns (QUAD_MEAN) and all returns above 2.5m (QUAD_MEAN_C)
CV, CV_C	Coefficient of variation for heights of all returns (CV) and all returns above 2.5m (CV_C)
L2, L3, L4, L_CV, L_SKEW, L_KURT	L-moments and their ratios as defined by Hosking (1990), calculated for heights of all returns
CANCOV	Ratio of returns above 2.5m to all returns (Pflugmacher et al. 2012)
HVOL	CANCOV * ZMEAN (Pflugmacher et al. 2012)
RPC1	Ratio of first returns to all returns (Pflugmacher et al. 2012)

confound the impacts of ground noise filtering.

Each of these models were tuned separately using a standard uniform grid search, with each model evaluated using the same 8,892 combinations of hyperparameters detailed in Supplementary Materials S2. Models from this set were ranked on the basis of mean root mean squared error (RMSE) from 5-fold cross validation (Stone, 1974) (Equation (1)), with 5 folds chosen to reduce computational demands. In order to ensure the best model was chosen for each combination, the top 100 models as determined from 5-fold cross validation were then evaluated again using leave-one-out cross validation (Lachenbruch & Mickey, 1968), with the final model fit using the hyperparameter set with the lowest RMSE. This method ensured that each random forest compared is the best version of the model that could be fit to these predictors, with the intention that any difference in model performance will be due to ground noise filtering and not stochastic differences between models or effort spent in tuning hyperparameters. Recent work has suggested cross validation assessments of model accuracy are likely overoptimistic compared to actual predictive accuracy (Bates et al., 2021), which does not impact our aim of comparing ground noise filtering approaches within a single study, but should be kept in mind when assessing these models as AGB estimators in their own right.

All modeling work was done using R version 4.0.5 (R Core Team, 2021).

2.5. Model Assessment

Given the scarcity of field data available for some LiDAR regions, models were evaluated using multiple metrics calculated via leave-one-out cross validation (Lachenbruch & Mickey, 1968). Performance metrics calculated included root-mean-squared error both as a value in Mg ha^{-1} (RMSE, Equation (1)) and as a percentage of mean plot AGB (RMSE %, Equation (2)), mean absolute error (MAE, Equation (3)), and the coefficient of determination (R^2, Equation (4)).

$$\text{RMSE} = \sqrt{(\frac{1}{n})\sum_{i=1}^{n}(y_i - \hat{y_i})^2} \tag{1}$$

$$\text{RMSE }\% = 100 \cdot \frac{\text{RMSE}}{\bar{y}} \tag{2}$$

$$\text{MAE} = (\frac{1}{n})\sum_{i=1}^{n}|y_i - \hat{y_i}| \tag{3}$$

$$\text{R}^2 = 1 - \frac{\sum_{i=1}^{n}(y_i - \hat{y_i})^2}{\sum_{i=1}^{n}(y_i - \bar{y})^2} \tag{4}$$

Where n is the number of FIA plots included in the data set, $\hat{y_i}$ is the predicted value of AGB, y_i the AGB value measured at the corresponding location, and $\bar{y}$ the mean AGB value from FIA field measurements.

Given that these regions represent a diversity of landscapes, including both highly developed regions and large swaths of contiguous forest (Figure 2), we investigated how changes in model accuracy due to ground noise filtering varied with differences in landscape structure. Landscape structure was quantified for each LiDAR region using temporally matching land use/land cover classifications from USGS LCMAP (Brown et al., 2020). We computed the proportion of pixels classified as forest (Equation (5)), as well as edge density (Equation (6)) in units of meter per hectare and patch density (Equation (7)) in units of number of patches per 100 hectares for each individual LiDAR region using the landscapemetrics R package (Hesselbarth et al., 2019; McGarigal & Marks, 1995).

$$\text{Forest Cover }\% = \frac{F}{A} \tag{5}$$

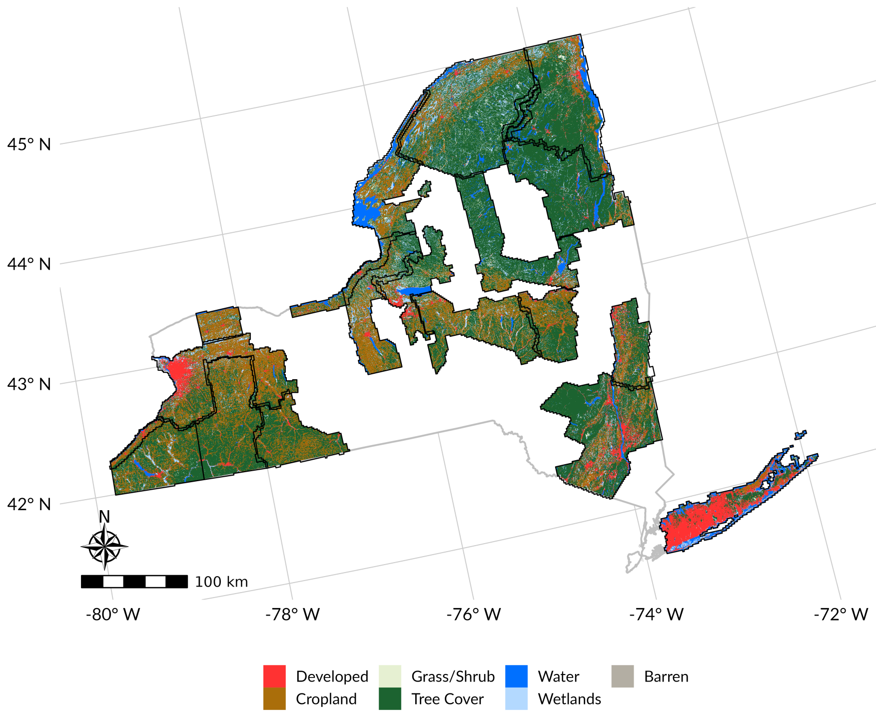

Figure 2: Land cover classifications across LiDAR regions, using land cover classifications from LCMAP (Brown et al., 2020). Lines represent LiDAR data set boundaries.

$$\text{Edge Density} = \frac{E}{A} \cdot 10000 \tag{6}$$

$$\text{Patch Density} = \frac{N}{A} \cdot 10000 \cdot 100 \tag{7}$$

Where F is the area classified as forest in square meters, A the total landscape area in square meters, E the total landscape edge in meters, and N the number of patches in the region.

The relationship between changes in model accuracy due to ground noise filtering and landscape structure was measured using Spearman's correlation coefficient (ρ).

3. Results

3.1. Landscape Structure

Edge density ranged from 38.73 to 100.17 meters per hectare, patch density from 8.63 to 23.70 patches per 100 hectares, and forest coverage from 15.38% to 83.29% of each LiDAR region (Figure 3). LiDAR regions had between 9 and 126 FIA plots available for models after applying plot inclusion rules, for a total of 874 plots in the combined data set (Table 3).

3.2. Variable Distribution

Filtering out ground noise resulted in shifts in predictor distributions (Figure 4). Filtering returns based upon z-thresholds or ground classifications resulted in systematically elevated height percentile and return density predictors (the H and D prefixed predictors in Table 1; Figure 4), with differences persisting into the highest percentiles. Notable differences in distributions also existed for all L-moment based predictors, with increasing height thresholds associated with increased magnitude of difference. Mean predictor values for each ground noise filtering method, alongside Kolmogorov-Smirnov test statistic values comparing the distributions of filtered predictors to that of the unfiltered predictors, are presented in Supplementary Materials S3.

Shifts in predictor distributions resulted in changes to covariance among variables, as measured via Spearman correlation coefficients. More aggressive filtering approaches were generally associated with stronger positive correlations and collinearity between all variables (Figure 5).

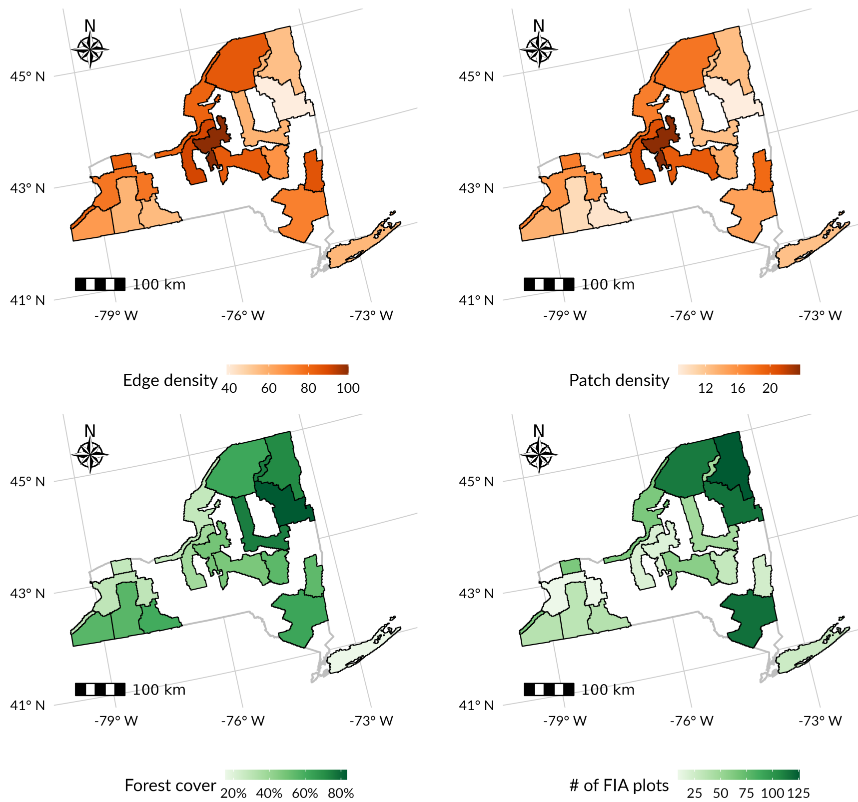

Figure 3: Landscape fragmentation metrics, derived from LCMAP LULC classifications for all LiDAR regions used in this project at year of LiDAR acquisition, and number of FIA plots available for modeling after inclusion rules within each coverage.

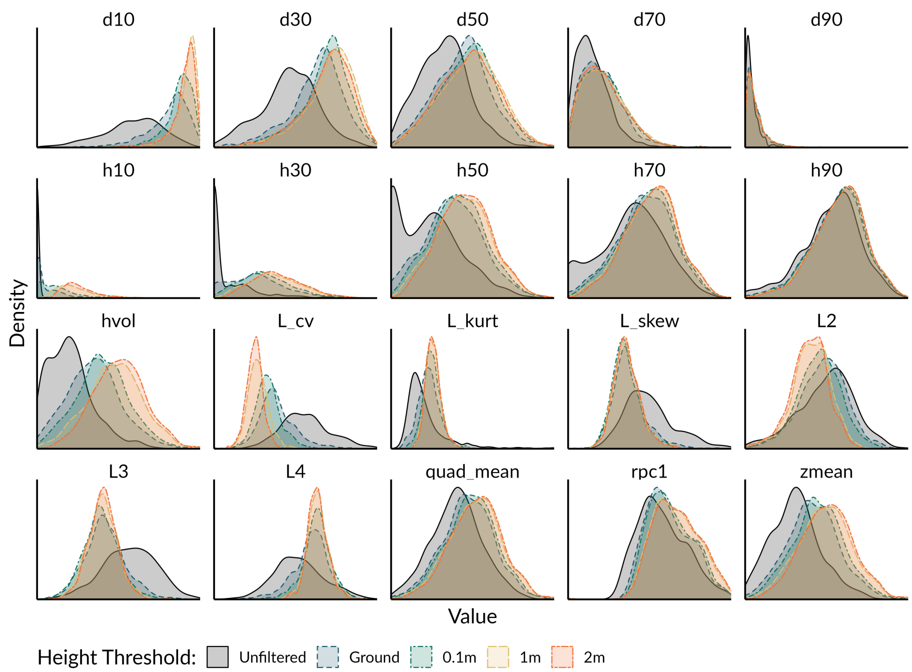

Figure 4: Selected LiDAR-derived predictor distributions for five ground noise filtering approaches, using all LiDAR regions combined. Each subplot is scaled independently so that the X-axis represents the full range of that predictor and the Y-axis represents the full range of the kernel density estimate of that predictor.

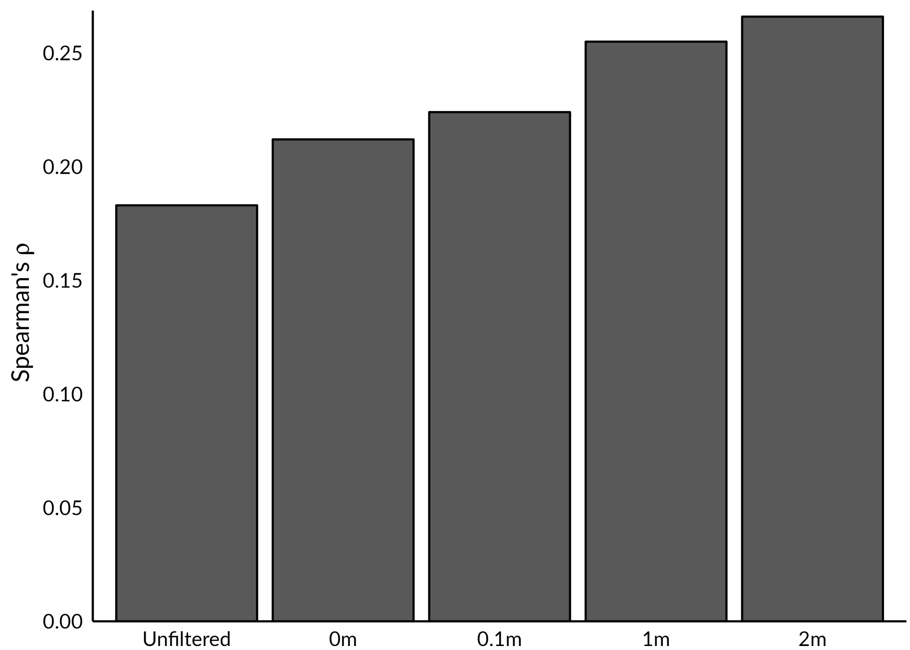

Figure 5: Mean Spearman correlation coefficients between LiDAR-derived variables calculated from point clouds processed with five different ground noise filtering methodologies across the combined data set. Variables with standard deviations of 0 after filtering (such as when minimum return height at all plots became 0 due to ground noise filtering) were excluded from calculations.

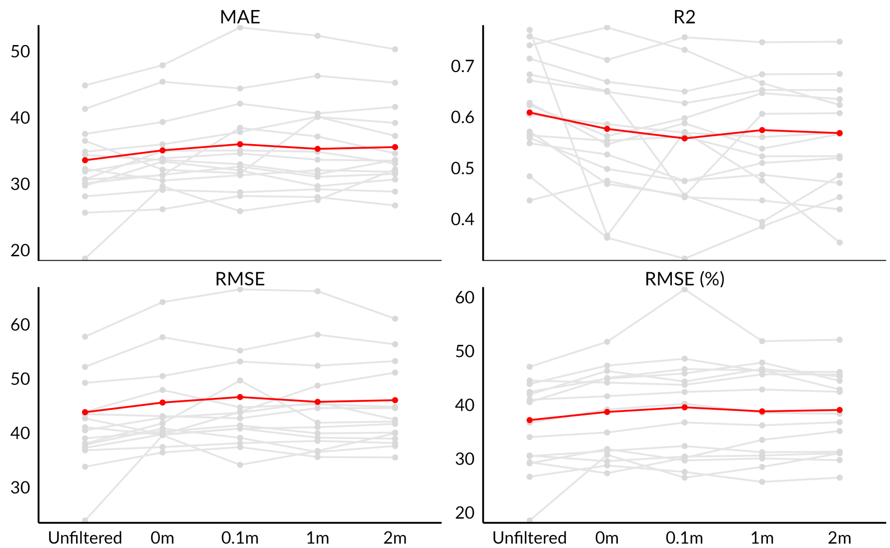

Figure 6: Model accuracy metrics at each ground noise filtering height threshold. Red line indicates models fit to all LiDAR regions (874 FIA plots), while grey lines represent each individual LiDAR region model with more than 10 FIA plots. Metrics are defined in Section 2.5.

3.3. Model Performance

Models fit to the unfiltered set of predictors were almost always equally or more accurate than those fit to predictors derived from filtered point clouds (Figure 6, Table 2, Table 3). Model accuracy generally decreased as filtering thresholds increased, with RMSE % for models fit to all regions combined increasing from 37.18% when using the unfiltered data set to 39.06% when using a threshold of 2 meters (Figure 6). An exception to this pattern was the Erie, Genesee, & Livingston LiDAR region, which saw improvements in accuracy with filtering procedures; this is likely related to the small sample size available for this region (with only 9 FIA plots available for models) making this region highly susceptible to small changes in the predictor space or hyperparameter space.

Model accuracy was impacted most by filtering when the area mapped was highly fragmented or contained large tracts of non-forested land (Table

Table 2: Model accuracy metrics for the model fit to the combined data set at various ground filtering height thresholds. The complete set of model accuracy metrics for all LiDAR regions is included as Supplementary Materials S4.

	Unfiltered	0m	0.1m	1m	2m
RMSE	43.826	45.608	46.622	45.734	46.044
RMSE (%)	37.177	38.689	39.548	38.795	39.058
MAE	33.560	35.048	35.974	35.271	35.540
R2	0.609	0.577	0.558	0.574	0.568

4). Increasing edge and patch densities were both positively correlated with Δ RMSE following ground noise filtering, indicating greater increases in RMSE after filtering in more heterogenous landscapes, while increasing forest cover was negatively correlated with Δ RMSE (Table 4).

4. Discussion

This study set out to evaluate empirical support for threshold-based ground noise filtering for models of forest AGB. We found that this common practice results in worse models of AGB, with lower predictive accuracy across multiple combinations of LiDAR regions and filtering thresholds representing a broad spectrum of landscape structures. While filtering had minimal impact on predictive accuracy in the most contiguously forested regions, the increasing research focus on large-scale "wall-to-wall" biomass mapping and potential for decreased accuracy following filtering procedures should encourage future modeling studies to use unfiltered point clouds when deriving variables for AGB models.

4.1. Ground noise filtering produces inferior predictive models

Our study demonstrates that the ground noise filtering approaches commonly used in preprocessing data for models of AGB systematically biases LiDAR-derived variables, with an end result being inferior models that produce less

Table 3: RMSE for each LiDAR region at various ground filtering height thresholds. The complete set of model accuracy metrics for all LiDAR regions is included as Supplementary Materials S4.

		RMSE				
Region	# Plots	Unfiltered	0m	0.1m	1m	2m
All Regions	874	43.826	45.608	46.622	45.734	46.044
Allegany & Steuben	38	43.478	43.102	42.702	44.589	44.577
3 County	117	49.238	50.479	53.164	52.394	53.238
Cayuga & Oswego	19	23.873	39.584	34.126	36.687	39.947
Clinton, Essex & Franklin	126	37.255	39.742	40.821	39.135	38.952
Columbia & Rensselaer	23	42.689	39.721	43.885	48.731	51.126
Erie, Genesee & Livingston	9	56.942	51.461	30.960	32.279	49.731
Franklin & St. Lawrence	113	36.818	37.411	38.121	38.538	38.143
Fulton, Saratoga, Herkimer & Franklin	47	37.840	40.823	39.105	36.496	37.610
Great Lakes	64	33.790	36.419	37.395	35.569	35.497
Long Island	26	38.047	41.796	49.667	41.893	42.107
Madison & Otsego	58	39.014	40.252	41.412	39.937	40.072
Oneida Subbasin	17	40.490	42.839	43.741	45.677	42.455
Schoharie	30	52.186	57.639	55.185	58.110	56.344
Southwest (spring)	37	43.921	47.921	44.715	45.297	44.806
Southwest (fall)	34	57.744	64.114	66.464	66.126	61.060
Warren, Washington & Essex	116	41.072	39.656	40.816	41.054	41.678

Table 4: Correlation (Spearman's ρ) between Δ RMSE (%) and landscape structural metrics at various filtering thresholds. Δ RMSE (%) represents the difference between RMSE (%) for the filtered scenario compared to RMSE (%) without filtering; positive correlations represent error increasing as the landscape metric increases. The negative correlation with increasing forest cover implies that areas with less forest are more negatively impacted by filtering; it is not generally the case that contiguously forested landscapes are positively impacted.

Filtering threshold	Edge density	Patch density	% Forest cover
0m	0.026	0.056	-0.368
0.1m	0.141	0.218	-0.382
1m	0.365	0.332	-0.388
2m	0.321	0.326	-0.388

accurate predictions than models fit on unfiltered data sets (Figure 4, Figure 6, Table 2). Increasing intensity of ground noise filtering was generally, but not universally, associated with worse model performance (Table 2, 3). These patterns were generally stronger as landscape fragmentation increased, with the correlation between model errors and landscape fragmentation increasing as filtering intensity increased.

These results are intuitive when thinking about the actual stand characteristics that may lead to an abundance or lack of ground returns. Dense forest stands making full use of the available light should be expected to have fewer returns reaching below the uppermost branches, while regions with many gaps in the canopy will have more such returns. If we conceive of our returns as providing information about the height structure of the stand as a whole, rather than about individual trees, it stands to reason that variables calculated using all returns are more informative about stand metrics such as AGB than those using filtered point clouds which may sacrifice information about stand openness. This could explain the impact of ground noise filtering seen in this study using leaf-off LiDAR; we might expect this impact to be even more pronounced were we to use leaf-on LiDAR in its place.

Our results also make sense mechanistically given the properties of the random forest algorithm used to construct AGB models in this study. Random forests excel at predicting outcomes based upon the consensus of weak learners (Breiman, 2001), individual decision trees which themselves rely upon small and ephemeral correlations between predictor variables and the outcome of interest. As shown in Figure 5, ground noise filtering approaches increase positive correlations between predictor variables, with the resulting increased collinearities shrinking the number and magnitude of possible weak correlations between individual variables and AGB (Langford et al., 2001). While the decision trees comprising the random forest may be able to take advantage of the correlations between predictor variables and the outcome to achieve similar accuracy as when trained on unfiltered data sets, we would not expect that a process that uniformly increases the positive linear correlation between variables would be associated with improved predictions.

Insights drawn from these results may not be limited to only machine learning based models. Anderson and Bolstad (2013) briefly note that, when fitting linear models to predict AGB, models based on unfiltered point clouds always provided better results than those fit to predictors calculated using only returns above 2 meters. However, few other AGB modeling studies have performed similar investigations, necessitating our current study. Our conclusions may not apply to AGB models of non-forest systems; investigations of ground noise filtering as a preprocessing step for models of corn AGB found improvements in predictive accuracy with relatively low height thresholds (Luo et al., 2016), emphasizing that commonly accepted data processing practices cannot be assumed to transfer across systems or domains to new questions of interest.

4.2. Differences between regional models

Although we found that models fit using predictors derived from unfiltered point clouds to be the most consistently accurate, the degree to which ground noise filtering damaged predictive accuracy and the relationship between filtering intensity and accuracy varied between regions. More fragmented landscapes tended to be more impacted by ground noise filtering, with model error increasing the most in landscapes with greater patch and edge densities and less forest cover (Table 4). These regions are characterized by large amounts of marginal forestland, resulting in a higher proportion of plots with low AGB and lower mean AGB values compared to more contiguously forested regions. As a result, it stands to reason that more returns in these highly fragmented landscapes are affected by the filtering procedure, removing more information from the model and resulting in inferior predictions.

4.3. Limitations as AGB models

The models discussed in this study were fit using only LiDAR-derived predictors so as to maximize the potential effect of ground noise filtering on model performance, as predictors obtained from additional data sources may be correlated with unfiltered predictors and as such used in their place by the random forest algorithm (Efron, 2020), mediating the impact of filtering. Additionally, these models were fit using extensive hyperparameter tuning performed via an automated process so as to avoid unintentionally biasing results by giving different models differing levels of attention or time in tuning. This process ensures that our models can be directly compared without worrying about a human “thumb on the scale,” but might result in models which fail to generalize beyond the training data due to the extensive tuning process. Further, model assessment was done using leave-one-out cross validation, which is sufficient for comparison between individual models but lacking as a way to characterize model AGB predictions spatially and across multiple scales (Riemann et al., 2010). While none of these limitations impact the comparison of ground noise filtering approaches at the center of this study, in combination they prevent us from using these models to make fine-scale estimates about AGB stocks across these regions and how model predictions compare to regional FIA estimates.

4.4. Recommendations for future models

Our results and examination of the literature suggest that ground noise filtering procedures are not well justified for studies modeling AGB, given both the potential information lost about stand density and structure, and the empirical inferiority of models fit using predictors derived from filtered point clouds. We make no such claim about researchers modeling other variables using LiDAR-derived predictors. For instance, the procedure likely makes sense when modeling mean tree heights similar to Næsset's (1997) study which originated the practice of ground noise filtering. The best data preprocessing procedure will necessarily depend on the purpose of the model (Sambasivan et al., 2021).

More generally, this study offers a reminder that all data preprocessing steps should be well justified in the context of any new analytical workflow. While tracing methodological details to their origins in the literature may not always be fruitful, researchers should ideally have the ability to separate out small sections of their data to evaluate model performance with and without the proposed procedure. The results of these small tests may justify including the procedure in the data preprocessing workflow for the full data set, or alternately lead a team to remove a processing step to save data cleaning time without damaging predictive accuracy. In these early days of big data in environmental science, we remain wanting for a cohesive theory of optimal prediction (Efron, 2020); as a result, beliefs about methodological improvements are still best tested by experiment.

5. Conclusion

Our study demonstrates that preprocessing LiDAR point clouds to filter out ground noise may be detrimental when making predictions of above-ground biomass using machine learning methods. This impact is particularly notable within mixed-use and otherwise heterogeneous landscapes, given the increased proportion of ground returns recorded when mapping these areas compared to contiguously forested regions. Although well-justified in its original context of modeling mean stand heights, the persistence of ground noise filtering in LiDAR-based AGB modeling appears to produce less accurate predictions than could be achieved using currently available data.

6. Acknowledgements

We would like to thank the US Forest Service Forest Inventory & Analysis program for their data sharing and cooperation, the New York State GIS Program Office for compiling LIDAR data, and the New York State Department of Environmental Conservation, Office of Climate Change, for funding support.

7. Conflict of Interest

The authors declare that they have no conflicting interests.

8. Authors' Contributions

MM, LJ, and CB conceived the ideas and designed methodology; MM, LJ, EB, and CB analysed the data; MM led the writing of the manuscript. All authors contributed critically to the drafts and gave final approval for publication.

9. Data Availability Statement

Data available from the Dryad Digital Repository https://doi.org/10.5061/dryad.t1g1jwt47 (Mahoney et al., 2022).

References

Anderson, R. S., & Bolstad, P. V. (2013). Estimating Aboveground Biomass and Average Annual Wood Biomass Increment with Airborne Leaf-on and Leaf-off LiDAR in Great Lakes Forest Types. *Northern Journal of Applied Forestry*, *30*(1), 16–22. https://doi.org/10.5849/njaf.12-015

Bates, S., Hastie, T., & Tibshirani, R. (2021). *Cross-validation: What does it estimate and how well does it do it? arXiv:2104.00673v2 [stat.ME]*. https://arxiv.org/abs/2104.00673

Breiman, L. (2001). Random Forests. *Machine Learning*, *45*, 5–32. https://doi.org/10.1023/A:1010933404324

Brown, J. F., Tollerud, H. J., Barber, C. P., Zhou, Q., Dwyer, J. L., Vogelmann, J. E., Loveland, T. R., Woodcock, C. E., Stehman, S. V., Zhu, Z., Pengra, B. W., Smith, K., Horton, J. A., Xian, G., Auch, R. F., Sohl, T. L., Sayler, K. L., Gallant, A. L., Zelenak, D., ... Rover, J. (2020). Lessons learned implementing an operational continuous united states national land change monitoring capability: The land change monitoring, assessment, and projection (LCMAP) approach. *Remote Sensing of Environment*, *238*, 111356. https://doi.org/10.1016/j.rse.2019.111356

Deo, R. K., Russell, M. B., Domke, G. M., Andersen, H.-E., Cohen, W. B., & Woodall, C. W. (2017). Evaluating site-specific and generic spatial models of aboveground forest biomass based on landsat time-series and LiDAR strip samples in the eastern USA. *Remote Sensing*, *9*(6). https://doi.org/10.3390/rs9060598

Dubayah, R. O., & Drake, J. B. (2000). Lidar remote sensing for forestry. *Journal of Forestry*, *98*(6), 44–46. https://doi.org/10.1093/jof/98.6.44

Efron, B. (2020). Prediction, estimation, and attribution. *Journal of the American Statistical Association*, *115*(530), 636–655. https://doi.org/10.

1080/01621459.2020.1762613

García, M., Riaño, D., Chuvieco, E., & Danson, F. M. (2010). Estimating biomass carbon stocks for a mediterranean forest in central spain using LiDAR height and intensity data. *Remote Sensing of Environment*, *114*(4), 816–830. https://doi.org/10.1016/j.rse.2009.11.021

Gray, A. N., Brandeis, T. J., Shaw, J. D., McWilliams, W. H., & Miles, P. (2012). Forest inventory and analysis database of the United States of America (FIA). *Biodiversity and Ecology*, *4*, 225–231. https://doi.org/10.7809/b-e.00079

Hawbaker, T. J., Gobakken, T., Lesak, A., Trømborg, E., Contrucci, K., & Radeloff, V. (2010). Light detection and ranging-based measures of mixed hardwood forest structure. *Forest Science*, *56*(3), 313–326. https://doi.org/10.1093/forestscience/56.3.313

Hesselbarth, M. H. K., Sciaini, M., With, K. A., Wiegand, K., & Nowosad, J. (2019). landscapemetrics: An open-source R tool to calculate landscape metrics. *Ecography*, *42*, 1648–1657.

Hosking, J. R. M. (1990). L-moments: Analysis and estimation of distributions using linear combinations of order statistics. *Journal of the Royal Statistical Society. Series B (Methodological)*, *52*(1), 105–124. http://www.jstor.org/stable/2345653

Huang, W., Dolan, K., Swatantran, A., Johnson, K., Tang, H., O'Neil-Dunne, J., Dubayah, R., & Hurtt, G. (2019). High-resolution mapping of aboveground biomass for forest carbon monitoring system in the Tri-State region of Maryland, Pennsylvania and Delaware, USA. *Environmental Research Letters*, *14*(9), 095002. https://doi.org/10.1088/1748-9326/ab2917

Hudak, A. T., Fekety, P. A., Kane, V. R., Kennedy, R. E., Filippelli, S. K., Falkowski, M. J., Tinkham, W. T., Smith, A. M. S., Crookston, N. L., Domke, G. M., Corrao, M. V., Bright, B. C., Churchill, D. J., Gould, P. J., McGaughey,

R. J., Kane, J. T., & Dong, J. (2020). A carbon monitoring system for mapping regional, annual aboveground biomass across the northwestern USA. *Environmental Research Letters*, *15*(9), 095003. https://doi.org/10.1088/1748-9326/ab93f9

Lachenbruch, P. A., & Mickey, M. R. (1968). Estimation of error rates in discriminant analysis. *Technometrics*, *10*(1), 1–11. https://doi.org/10.2307/1266219

Langford, E., Schwertman, N., & Owens, M. (2001). Is the property of being positively correlated transitive? *The American Statistician*, *55*(4), 322–325. https://doi.org/10.1198/000313001753272286

Luo, S., Chen, J. M., Wang, C., Xi, X., Zeng, H., Peng, D., & Li, D. (2016). Effects of LiDAR point density, sampling size and height threshold on estimation accuracy of crop biophysical parameters. *Opt. Express*, *24*(11), 11578–11593. https://doi.org/10.1364/OE.24.011578

Ma, W., Domke, G. M., D'Amato, A. W., Woodall, C. W., Walters, B. F., & Deo, R. K. (2018). Using matrix models to estimate aboveground forest biomass dynamics in the eastern USA through various combinations of LiDAR, landsat, and forest inventory data. *Environmental Research Letters*, *13*(12), 125004. https://doi.org/10.1088/1748-9326/aaeaa3

Magnussen, S., & Boudewyn, P. (1998). Derivations of stand heights from airborne laser scanner data with canopy-based quantile estimators. *Canadian Journal of Forest Research*, *28*(7), 1016–1031. https://doi.org/10.1139/x98-078

Mahoney, M. J., Johnson, L. K., Bevilacqua, E., & Beier, C. M. (2022). *Data from: Filtering ground noise from LiDAR returns produces inferior models of forest aboveground biomass.* https://doi.org/10.5061/dryad.t1g1jwt47

Massey, F. J. (1951). The Kolmogorov-Smirnov test for goodness of fit. *Journal *of the American Statistical Association*, *46*(253), 68–78. https://doi.org/10.1080/01621459.1951.10500769

McGarigal, K., & Marks, B. J. (1995). FRAGSTATS: Spatial pattern analysis program for quantifying landscape structure. *Gen. Tech. Rep. PNW-GTR-351. Portland, OR: US Department of Agriculture, Forest Service, Pacific Northwest Research Station. 122 p*, *351*.

Næsset, E. (1997). Determination of mean tree height of forest stands using airborne laser scanner data. *ISPRS Journal of Photogrammetry and Remote Sensing*, *52*(2), 49–56. https://doi.org/10.1016/S0924-2716(97)83000-6

Nilsson, M. (1996). Estimation of tree heights and stand volume using an airborne lidar system. *Remote Sensing of Environment*, *56*(1), 1–7. https://doi.org/10.1016/0034-4257(95)00224-3

Nilsson, M., Nordkvist, K., Jonzén, J., Lindgren, N., Axensten, P., Wallerman, J., Egberth, M., Larsson, S., Nilsson, L., Eriksson, J., & Olsson, H. (2017). A nationwide forest attribute map of sweden predicted using airborne laser scanning data and field data from the national forest inventory. *Remote Sensing of Environment*, *194*, 447–454. https://doi.org/10.1016/j.rse.2016.10.022

Pflugmacher, D., Cohen, W. B., & Kennedy, R. E. (2012). Using landsat-derived disturbance history (1972–2010) to predict current forest structure. *Remote Sensing of Environment*, *122*, 146–165. https://doi.org/10.1016/j.rse.2011.09.025

Pflugmacher, D., Cohen, W. B., Kennedy, R. E., & Yang, Z. (2014). Using landsat-derived disturbance and recovery history and lidar to map forest biomass dynamics. *Remote Sensing of Environment*, *151*, 124–137. https://doi.org/10.1016/j.rse.2013.05.033

R Core Team. (2021). *R: A language and environment for statistical computing.*

R Foundation for Statistical Computing. https://www.R-project.org/

Riemann, R., Wilson, B. T., Lister, A., & Parks, S. (2010). An effective assessment protocol for continuous geospatial datasets of forest characteristics using USFS forest inventory and analysis (FIA) data. *Remote Sensing of Environment*, *114*(10), 2337–2352. https://doi.org/10.1016/j.rse.2010.05.010

Roussel, J.-R., Auty, D., Coops, N. C., Tompalski, P., Goodbody, T. R. H., Meador, A. S., Bourdon, J.-F., de Boissieu, F., & Achim, A. (2020). lidR: An R package for analysis of airborne laser scanning (ALS) data. *Remote Sensing of Environment*, *251*, 112061. https://doi.org/10.1016/j.rse.2020.112061

Sambasivan, N., Kapania, S., Highfill, H., Akrong, D., Paritosh, P., & Aroyo, L. (2021). "Everyone wants to do the model work, not the data work": Data cascades in high-stakes AI. *Proceedings of CHI 2021*.

Stone, M. (1974). Cross-validatory choice and assessment of statistical predictions. *Journal of the Royal Statistical Society. Series B (Methodological)*, *36*(2), 111–147. http://www.jstor.org/stable/2984809

Wasser, L., Day, R., Chasmer, L., & Taylor, A. (2013). Influence of vegetation structure on lidar-derived canopy height and fractional cover in forested riparian buffers during leaf-off and leaf-on conditions. *PLOS ONE*, *8*(1), 1–13. https://doi.org/10.1371/journal.pone.0054776

White, J. C., Arnett, J. T. T. R., Wulder, M. A., Tompalski, P., & Coops, N. C. (2015). Evaluating the impact of leaf-on and leaf-off airborne laser scanning data on the estimation of forest inventory attributes with the area-based approach. *Canadian Journal of Forest Research*, *45*(11), 1498–1513. https://doi.org/10.1139/cjfr-2015-0192

Wright, M. N., & Ziegler, A. (2017). ranger: A fast implementation of random forests for high dimensional data in C++ and R. *Journal of Statistical Software*, *77*(1), 1–17. https://doi.org/10.18637/jss.v077.i01

Supplementary Materials

Contents

1 S1: LiDAR data sets

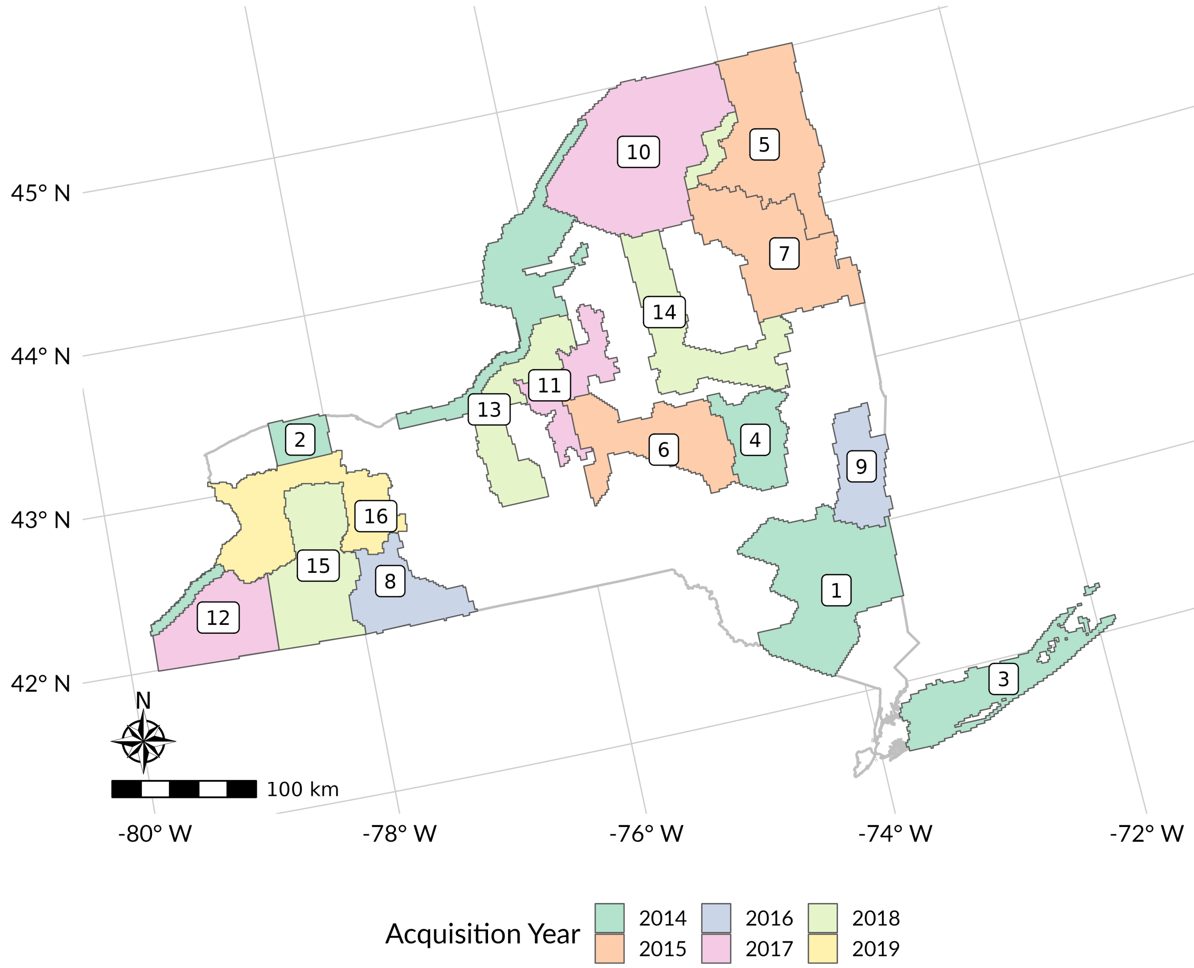

Figure 1: Boundaries for all LiDAR coverages used in this project, colored by year of data acquisition. Numbers on each coverage represent the "index" value of that coverage in table Supplementary Materials S1.

Table 1: Lidar region characteristics. "Index" numbers reflect identifier numbers as used in Supplementary Materials Figure 1. Region names reflect the naming conventions used by the NYSGPO; this often, but not always, reflects included counties. Area values are approximate and in square kilometers. Density values are in points per square meter (ppm^2). Edge density is in units of meters per hectare, and patch density in number of patches per 100 hectares.

Index	Region Name	Acquisition Year	Area	Density	Edge Density	Patch Density	Forest Cover	Citation
1	3 County	2014	7,370	2.04	73.20	14.63	62.57%	United States Geological Survey (2015a)
2	Great Lakes	2014	5,780	2.04	81.24	17.23	27.77%	United States Geological Survey (2015c)
3	Long Island	2014	3,170	2.04	56.57	12.34	15.38%	Woolpert, Inc (2014)
4	Schoharie	2014	2,500	2.04	67.48	13.60	54.95%	United States Geological Survey (2015b)
5	Clinton, Essex & Franklin	2015	1,110	2.04	54.03	12.49	71.94%	Quantum Spatial (2016)
6	Madison & Otsego	2015	4,780	2.18	83.99	19.76	47.73%	Axis GeoSpatial, LLC (2016a)
7	Warren, Washington & Essex	2015	6,280	3.24	38.73	8.63	83.29%	Atlantic Inc (2015)
8	Allegany & Steuben	2016	3,410	2.04	55.41	9.39	60.50%	New York Office of Information Technology Services (2016)
9	Columbia & Rensselaer	2016	2,600	2.60	86.36	18.62	54.18%	Axis GeoSpatial, LLC (2016b)
10	Franklin & St. Lawrence	2017	9,880	2.04	84.66	17.84	62.14%	Quantum Spatial (2017b)
11	Oneida Subbasin	2017	2,550	2.04	100.17	23.70	49.09%	Quantum Spatial (2017a)
12	Southwest (spring)	2017	4,460	2.04	65.44	13.40	55.76%	New York Office of Information Technology Services (2017)
13	Cayuga & Oswego	2018	4,450	2.04	90.75	20.55	37.86%	New York Office of Information Technology Services (2018a)
14	Fulton, Saratoga, Herkimer & Franklin	2018	5,010	1.98	57.74	12.31	75.21%	Quantum Spatial (2018)

Table 1: Lidar region characteristics. "Index" numbers reflect identifier numbers as used in Supplementary Materials Figure 1. Region names reflect the naming conventions used by the NYSGPO; this often, but not always, reflects included counties. Area values are approximate and in square kilometers. Density values are in points per square meter (ppm^2). Edge density is in units of meters per hectare, and patch density in number of patches per 100 hectares. *(continued)*

Index	Region Name	Acquisition Year	Area	Density	Edge Density	Patch Density	Forest Cover	Citation
15	Southwest (fall)	2018	5,660	2.04	57.52	10.20	55.74%	New York Office of Information Technology Services (2018b)
16	Erie, Genesee & Livingston	2019	5,670	2.04	76.19	15.69	29.22%	New York Office of Information Technology Services (2019)

2 S2: List of hyperparameters used in tuning random forests and evaluated ranges

Table 2: List of hyperparameters used in tuning random forests and evaluated ranges. Models were tuned using a uniform grid containing all combinations of all values of all variables save num.trees, which was tuned separately.

Hyperparameter	Definition	Evaluated Range
mtry	Number of variables to include in each node	Integers between 3 and 40
min.node.size	The minimum number of observations per terminal node	Integers between 3 and 15
sample.fraction	Fraction of observations to sample	0.2 to 1.0 in increments of 0.1
replace	Whether or not to sample with replacement	TRUE and FALSE
num.trees	Number of trees to aggregate	100 to 2000 in increments of 100. Tuned separately from other hyperparameters for only the best performing model given that performance tends to improve with additional trees, independent of other parameter values.

3 S3: Mean values of LiDAR-derived variables and Kolmogorov-Smirnov test statistic values (in parentheses).

Table 3: Mean values of LiDAR-derived variables and Kolmogorov-Smirnov test statistic values (in parentheses) for the combined data set. Variables calculated for plots with no returns following filtering were set to 0, which may result in counterintuitive comparisons.

	0.1m	Ground	1m	2m	Unfiltered
cancov	0.868 (0.722)	0.799 (0.538)	0.951 (0.886)	0.997 (0.994)	0.586
cv	0.575 (0.716)	0.683 (0.541)	0.464 (0.847)	0.428 (0.897)	1.090
cv_c	0.407 (0.000)	0.407 (0.000)	0.407 (0.000)	0.407 (0.000)	0.407
d10	0.865 (0.732)	0.798 (0.565)	0.905 (0.810)	0.893 (0.799)	0.582
d20	0.770 (0.644)	0.712 (0.498)	0.802 (0.700)	0.789 (0.681)	0.522
d30	0.670 (0.568)	0.619 (0.442)	0.696 (0.600)	0.682 (0.574)	0.456
d40	0.564 (0.477)	0.521 (0.379)	0.582 (0.506)	0.568 (0.473)	0.384
d50	0.450 (0.397)	0.416 (0.317)	0.462 (0.414)	0.448 (0.389)	0.307
d60	0.329 (0.320)	0.304 (0.261)	0.335 (0.333)	0.322 (0.291)	0.224
d70	0.206 (0.260)	0.190 (0.209)	0.208 (0.260)	0.199 (0.232)	0.140
d80	0.098 (0.229)	0.090 (0.192)	0.099 (0.222)	0.094 (0.189)	0.066
d90	0.026 (0.199)	0.023 (0.165)	0.026 (0.195)	0.025 (0.176)	0.016
h10	2.409 (0.912)	1.361 (0.876)	4.448 (0.969)	5.040 (0.974)	0.156
h20	5.002 (0.783)	3.555 (0.652)	6.650 (0.864)	7.156 (0.891)	0.715
h30	7.224 (0.634)	5.867 (0.526)	8.537 (0.700)	8.968 (0.740)	1.885
h40	9.204 (0.514)	8.042 (0.411)	10.232 (0.574)	10.596 (0.606)	3.801
h50	10.998 (0.405)	10.107 (0.341)	11.801 (0.461)	12.114 (0.479)	6.164
h60	12.672 (0.301)	11.995 (0.246)	13.302 (0.346)	13.566 (0.360)	8.830
h70	14.334 (0.221)	13.803 (0.184)	14.813 (0.252)	15.031 (0.264)	11.383
h80	16.062 (0.166)	15.700 (0.135)	16.419 (0.191)	16.584 (0.205)	13.918
h90	18.095 (0.105)	17.842 (0.090)	18.324 (0.118)	18.430 (0.129)	16.722
h95	19.490 (0.082)	19.321 (0.068)	19.654 (0.090)	19.734 (0.095)	18.536
h99	21.510 (0.047)	21.422 (0.040)	21.596 (0.050)	21.634 (0.054)	21.036
hvol	9.526 (0.548)	8.281 (0.416)	11.229 (0.648)	11.938 (0.701)	4.875
L_cv	0.323 (0.723)	0.378 (0.546)	0.262 (0.854)	0.242 (0.903)	0.546
L_kurt	0.051 (0.457)	0.031 (0.325)	0.060 (0.526)	0.059 (0.539)	0.012
L_skew	-0.014 (0.466)	0.020 (0.406)	-0.005 (0.460)	-0.002 (0.457)	0.201
L2	3.271 (0.191)	3.448 (0.109)	2.930 (0.347)	2.830 (0.392)	3.585
L3	-0.086 (0.518)	0.006 (0.447)	-0.051 (0.532)	-0.043 (0.537)	0.542
L4	0.137 (0.457)	0.060 (0.324)	0.152 (0.526)	0.147 (0.540)	-0.090
max	23.413 (0.000)	23.413 (0.000)	23.412 (0.001)	23.410 (0.002)	23.413
min	0.104 (1.000)	0.005 (0.349)	1.077 (0.999)	2.030 (0.998)	0.000
n	3,872.788 (0.267)	4,178.778 (0.219)	3,543.318 (0.316)	3,423.683 (0.339)	5,471.683
quad_mean	12.197 (0.253)	11.711 (0.193)	12.754 (0.304)	12.976 (0.327)	10.027
quad_mean_c	13.122 (0.000)	13.122 (0.000)	13.122 (0.000)	13.122 (0.000)	13.122
rpc1	0.633 (0.189)	0.620 (0.152)	0.661 (0.255)	0.667 (0.272)	0.578
z_kurt	-0.583 (0.294)	-0.615 (0.193)	-0.513 (0.343)	-0.515 (0.352)	0.080
z_skew	-0.057 (0.408)	0.050 (0.352)	-0.015 (0.375)	0.002 (0.366)	0.589
zmean	10.667 (0.403)	9.879 (0.305)	11.608 (0.474)	11.942 (0.501)	7.374
zmean_c	12.151 (0.000)	12.151 (0.000)	12.151 (0.000)	12.151 (0.000)	12.151

4 S4: Model accuracy by LiDAR region

Table 4: RMSE for each LiDAR region at various ground filtering height thresholds.

Region	# Plots	RMSE				
		Unfiltered	0m	0.1m	1m	2m
All Regions	874	43.826	45.608	46.622	45.734	46.044
Allegany & Steuben	38	43.478	43.102	42.702	44.589	44.577
3 County	117	49.238	50.479	53.164	52.394	53.238
Cayuga & Oswego	19	23.873	39.584	34.126	36.687	39.947
Clinton, Essex & Franklin	126	37.255	39.742	40.821	39.135	38.952
Columbia & Rensselaer	23	42.689	39.721	43.885	48.731	51.126
Erie, Genesee & Livingston	9	56.942	51.461	30.960	32.279	49.731
Franklin & St. Lawrence	113	36.818	37.411	38.121	38.538	38.143
Fulton, Saratoga, Herkimer & Franklin	47	37.840	40.823	39.105	36.496	37.610
Great Lakes	64	33.790	36.419	37.395	35.569	35.497
Long Island	26	38.047	41.796	49.667	41.893	42.107
Madison & Otsego	58	39.014	40.252	41.412	39.937	40.072
Oneida Subbasin	17	40.490	42.839	43.741	45.677	42.455
Schoharie	30	52.186	57.639	55.185	58.110	56.344
Southwest (spring)	37	43.921	47.921	44.715	45.297	44.806
Southwest (fall)	34	57.744	64.114	66.464	66.126	61.060
Warren, Washington & Essex	116	41.072	39.656	40.816	41.054	41.678

Table 5: RMSE (%) for each LiDAR region at various ground filtering height thresholds.

Region	# Plots	RMSE (%)				
		Unfiltered	0m	0.1m	1m	2m
All Regions	874	37.18	38.69	39.55	38.80	39.06
Allegany & Steuben	38	44.52	44.13	43.73	45.66	45.64
3 County	117	34.02	34.88	36.74	36.21	36.79
Cayuga & Oswego	19	18.53	30.73	26.49	28.48	31.01
Clinton, Essex & Franklin	126	36.69	39.14	40.20	38.54	38.36
Columbia & Rensselaer	23	29.35	27.31	30.17	33.50	35.15
Erie, Genesee & Livingston	9	43.61	39.41	23.71	24.72	38.09
Franklin & St. Lawrence	113	40.95	41.61	42.40	42.86	42.43
Fulton, Saratoga, Herkimer & Franklin	47	26.66	28.76	27.55	25.71	26.49
Great Lakes	64	43.89	47.30	48.57	46.20	46.11
Long Island	26	47.08	51.71	61.45	51.83	52.10
Madison & Otsego	58	30.49	31.45	32.36	31.21	31.31
Oneida Subbasin	17	42.42	44.88	45.83	47.86	44.48
Schoharie	30	41.93	46.31	44.34	46.69	45.27
Southwest (spring)	37	29.15	31.81	29.68	30.06	29.74
Southwest (fall)	34	40.53	45.00	46.65	46.41	42.86
Warren, Washington & Essex	116	30.60	29.55	30.41	30.59	31.05

Table 6: MAE for each LiDAR region at various ground filtering height thresholds.

Region	# Plots	MAE				
		Unfiltered	0m	0.1m	1m	2m
All Regions	874	33.560	35.048	35.974	35.271	35.540
Allegany & Steuben	38	30.681	34.978	35.034	34.838	33.073
3 County	117	37.520	39.326	42.094	40.619	41.600
Cayuga & Oswego	19	18.721	29.625	25.873	27.545	32.179
Clinton, Essex & Franklin	126	30.068	31.358	32.594	31.056	31.495
Columbia & Rensselaer	23	36.475	32.143	31.581	40.088	39.186
Erie, Genesee & Livingston	9	47.617	46.599	24.948	27.124	41.119
Franklin & St. Lawrence	113	28.114	29.075	28.728	29.180	28.822
Fulton, Saratoga, Herkimer & Franklin	47	29.724	33.365	32.020	29.640	30.655
Great Lakes	64	25.647	26.167	28.175	27.999	26.735
Long Island	26	30.655	31.290	38.446	37.132	34.594
Madison & Otsego	58	31.842	33.841	34.575	33.633	33.480
Oneida Subbasin	17	34.843	35.944	37.813	40.118	37.229
Schoharie	30	41.306	45.392	44.386	46.290	45.248
Southwest (spring)	37	34.352	33.594	32.959	31.450	33.620
Southwest (fall)	34	44.847	47.884	53.584	52.324	50.291
Warren, Washington & Essex	116	32.257	30.497	31.295	32.056	31.800

Table 7: R2 for each LiDAR region at various ground filtering height thresholds.

Region	# Plots	R2				
		Unfiltered	0m	0.1m	1m	2m
All Regions	874	0.609	0.577	0.558	0.574	0.568
Allegany & Steuben	38	0.564	0.554	0.562	0.523	0.523
3 County	117	0.548	0.527	0.475	0.487	0.471
Cayuga & Oswego	19	0.771	0.367	0.571	0.475	0.354
Clinton, Essex & Franklin	126	0.559	0.498	0.474	0.510	0.519
Columbia & Rensselaer	23	0.740	0.775	0.731	0.666	0.624
Erie, Genesee & Livingston	9	0.544	0.657	0.883	0.871	0.650
Franklin & St. Lawrence	113	0.605	0.586	0.569	0.561	0.569
Fulton, Saratoga, Herkimer & Franklin	47	0.623	0.563	0.598	0.647	0.635
Great Lakes	64	0.714	0.669	0.650	0.684	0.684
Long Island	26	0.683	0.651	0.446	0.606	0.607
Madison & Otsego	58	0.672	0.649	0.627	0.653	0.653
Oneida Subbasin	17	0.571	0.469	0.446	0.394	0.485
Schoharie	30	0.628	0.546	0.588	0.538	0.567
Southwest (spring)	37	0.758	0.712	0.756	0.746	0.747
Southwest (fall)	34	0.484	0.363	0.323	0.385	0.443
Warren, Washington & Essex	116	0.437	0.475	0.443	0.437	0.419

References

Atlantic Inc. (2015). *NY_WarrenWashingtonEssex_Spring2015*. ftp://ftp.gis.ny.gov/elevation/LIDAR/.

Axis GeoSpatial, LLC. (2016a). *Axis GeoSpatial, LLC New York tiled LiDAR*. ftp://ftp.gis.ny.gov/elevation/LIDAR/.

Axis GeoSpatial, LLC. (2016b). *New York Office of Information Technology Services classified LiDAR tiles*. ftp://ftp.gis.ny.gov/elevation/LIDAR/.

New York Office of Information Technology Services. (2016). *Allegany and Steuben Counties, New York Lidar; overall project metadata*. ftp://ftp.gis.ny.gov/elevation/LIDAR/.

New York Office of Information Technology Services. (2017). *Southwest 17 - spring, New York Lidar; classified point cloud*. ftp://ftp.gis.ny.gov/elevation/LIDAR/.

New York Office of Information Technology Services. (2018a). *LIDAR collection (QL2) for Cayuga county and most of Oswego county, New York Lidar; classified point cloud*. ftp://ftp.gis.ny.gov/elevation/LIDAR/.

New York Office of Information Technology Services. (2018b). *Southwest 17-b - fall, New York Lidar; classified point cloud*. ftp://ftp.gis.ny.gov/elevation/LIDAR/.

New York Office of Information Technology Services. (2019). *LIDAR collection (QL2) for Erie, Genesee, and Livingston counties New York Lidar; classified point cloud*. ftp://ftp.gis.ny.gov/elevation/LIDAR/.

Quantum Spatial. (2016). *Clinton-Essex-Lake Champlain New York 2015 LiDAR USGS contract: G10PC00026 Task order number: G10PC00026 and G14PD000943 (modification) NY_ClintonEssex_2015*. ftp://ftp.gis.ny.gov/elevation/LIDAR/.

Quantum Spatial, Inc. (2017a). *New York FEMA 2016 QL2 LiDAR - Central zone AOI; classified point cloud*. ftp://ftp.gis.ny.gov/elevation/LIDAR/.

Quantum Spatial, Inc. (2017b). *New York FEMA 2016 QL2 LiDAR - East zone AOI; classified point cloud*. ftp://ftp.gis.ny.gov/elevation/LIDAR/.

Quantum Spatial, Inc. (2018). *Lidar collection (QL2) of all or part of Schuyler, Seneca, Steuben, Tompkins, Wayne and Yates counties, NY Lidar; classified point cloud*. ftp://ftp.gis.ny.gov/elevation/LIDAR/.

United States Geological Survey. (2015a). *LAS*. ftp://ftp.gis.ny.gov/elevation/LIDAR/.

United States Geological Survey. (2015b). *LAS*. ftp://ftp.gis.ny.gov/elevation/LIDAR/.

United States Geological Survey. (2015c). *LAS extents*. ftp://ftp.gis.ny.gov/elevation/LIDAR/.

Woolpert, Inc. (2014). *USGS Long Island New York Sandy Lidar classified LAS 1.2*. ftp://ftp.gis.ny.gov/elevation/LIDAR/.